# Solar Dryers in Passive Mode: Thermal Performance Evaluation

Karthikeyan Sathasivam#, ilhan GARIP *‡ , Hameed Hassan Khalaf ** , Waleed Mohammed Khazaal *** , Ahmed A. Ali **** , Kadhim A. Jabbar***** , Ahmed Read Al-Tameemi ****** , Ausama A. Almulla******* , Kadhum Al-Majdi********

#Department of Mechanical Engineering, Syed Ammal Engineering College, Tamilnadu, India

C*+ Department of Electrical and Electronics Engineering, Nisantasi University, Istanbul, Turkey
** Al-Manara College for Medical Sciences/ (Maysan)/Iraq
*** Mazaya University College/ Iraq
**** College of Petroleum Engineering, Al-Ayen University, Thi-Qar, Iraq
***** National University of Science and Technology, Dhi Qar, Iraq
****** Department of Biomedical Engineering/ AL-Nisour University College/ Baghdad/ Iraq
******* Al-Hadi University College, Baghdad, 10011, Iraq
******** Department of Biomedical Engineering/ Ashur University college/Baghdad/ Iraq
(karthikeyan@syedengg.ac.in, ilhangarip60@gmail.com, khalaf56125@gmail.com, khazaalbid@gmail.com, ahmed@hotmail.com, jabbar2024@hotmail.com, al-Tameemi67@gmail.com, ausama2024@gmail.com, al-majdi2024@gmail.com)

‡ Corresponding Author; ilhan GARIP, Department of Electrical and Electronics Eng., Nisantasi University, Istanbul, Turkey.

*Received: 12.01.2023 Accepted:12.01.2024*

**Abstract-** In this study, three solar dryers in a passive flow regime were evaluated for their thermal performance under the environmental conditions of the Colombian Caribbean Coast. In the field, experiments were conducted to determine the thermal efficiency of the structure. The results of field experiments were compared with those that were obtained from a computational simulation. Based on the energy balances in each of the dryer components, the simulation is based on the energy balances of each component. A simulation was carried out using specific open-source software using atmospheric data from the days when field tests were conducted. A consistent relationship is observed between the simulation results and the direct measurement results. The study emphasizes the importance of understanding and analyzing the thermal performance of solar dryers in a specific environmental context. By utilizing both direct measurements and computational simulations, the researchers aimed to provide a comprehensive evaluation of the solar dryers' efficiency under the given conditions. The observed consistent relationship between simulation results and direct measurements enhances the reliability and validity of the study's findings, emphasizing the effectiveness of the passive flow regime solar dryers in the Colombian Caribbean Coast environment

**Keywords:** Thermal model, Solar cooker, Cooking Power, Data centres, Thermal Performance

## 1. Introduction

The use of solar energy alone to produce hot air for dehydration in a sealed enclosure to prevent contamination with dust, insects, and rodents is crucial to maintain the quality of the product. The use of solar energy for producing hot air for product dehydration requires not only providing thermal power but also removing air using a current [1]. In addition to the constant airflow provided by pumps and fans, these devices require an additional source of power. The thermal balance of three air collector configurations in passive mode is proposed in this paper. A comparison of the heat balances and their thermal efficiency is conducted by comparing the results from testing on prototypes with the results from computational simulations [2]. A solar dryer has numerous advantages, although the main argument against them is the high initial cost of the construction, the auxiliary equipment, and the operating personnel. The advantages include a high amount of energy per unit of time available for evaporation, control of dehydration, no heat exposure, increased productivity, and application in different products [3]. The evaluation of the thermal performance of solar dryers lacks globally accepted standard methods. Many proposals have been prepared for the main focus on evaluation methodologies. A number of evaluation methods combining a variety of international standards are proposed

from the viewpoint of the absolute efficiency of the collector as an air heater. There is a proposal to add dryer characteristics such as cost, lifetime, installation, and maintenance. A dehydrator is evaluated based on its type, weight, dimensions, and materials of construction. Metal and wood are the most common, but cement and adobe are also used. Metal plates covered with matte black non-reflective paint and corrugated metal sheets are used for collectors, while selective materials are used for collectors requiring higher temperatures [4]. Transparent covers are usually made of glass or translucent materials such as polyvinyl fluoride, fluorinated ethylene polypropylene, tereheptalene polypropylene, polyethylene, and polycarbonate. Insulation materials include glass wool, rock wool, coconut fiber, sawdust agglomerate, hay, rice husk, and sawdust. The following three rules are adapted from Leon's proposal to improve and standardize the constructive conditions and to properly evaluate the performance of a dryer: (a) Average dehydrator load (4 kg of fresh product per square meter) (b) the collector area is multiplied by the tray area (0.75 times the tray area). c) Air flow (0.75 cubic meters per minute per square meter). Many contributions have been made in the literature for evaluating the energy efficiency of dryers. An analysis of the thermal efficiency of a dryer consisting of a collector and a drying chamber based on typical physical parameters [5]. The dryer was designed for use in arid regions of Turkey; the collection area consists of aluminium helical wires painted black as the absorption surface. The pre-heater was oriented southeast along with the drying chamber, and its angle was 30° (the latitude of the site). Polyether was used as the transparent surface and aluminium and stainless steel as the remaining materials; glass wool was used as insulation. An air fan controlled by manual speed drove the air. A temperature range of 30°C to 50°C was selected for the inlet temperatures. It was decided to use airflow values of 150, 200, and 250 kg/m2h for the selection of airflows. It was necessary to control the inlet temperature by using an electrical resistance. A minimum solar radiation of 630 W/m2 was recorded in the study [6]. According to the authors, the collector efficiency is defined as the useful heat divided by the total amount of radiation reaching the dryer. The useful heat is determined by evaluating the thermal power originated from the sensible heating of the airflow between the inlet and outlet of the dryer, while the total radiation is the product of the radiation of the airflow between the inlet and outlet of the dryer while the total radiation is the product of the radiation of the inlet and outlet of the dryer [7].

An analysis of the results shows a linear relationship between instantaneous efficiency and a parameter defined as the difference between the inlet-outlet temperatures and ambient temperatures divided by useful heat. The results are presented as a linear fit between the instantaneous efficiency and a parameter defined as the difference between the promised inlet outlet temperatures and the ambient temperature, all divided by the useful heat. The slopes are negative and steepen as the airflow decreases. According to [8], three different types of collectors were tested to determine which of the designs was the most suitable for use in solar drying based on the requirements of the ASHRAE standard for solar drying. It was different in their design because they changed the shape of the heat exchange surface within the collector. They used three types of collector sheet for each flow condition, flat, finned, and corrugated with v-waves, in order to modify the surface temperature. It was the latter design that proved to be the most efficient. The lamellae were recirculated with air to increase efficiency. The new methodology revealed that flat plate designs are the most efficient, whereas single air passage designs were found to be inefficient. Inlet-outlet temperatures were incremented by four different factors during the testing [9]. It was maintained that the amount of irradiation did not fall below 790 W/m2. Efficiency is calculated as the quotient of useful power and total power. A function of both mass flow and temperature difference between the collector's inlet and outlet was used to calculate how much heat was needed to heat the air of heat capacity Cp. Based on the area of the collector Ac and the amount of irradiation received by IT, the total amount of energy received was estimated. Air collectors are described by the Hottel-Willier-Bliss equation (2).

$$\eta = \frac{\dot{m}c_p \int_{t_1}^{t_2}(T_O - T_i)dt}{A_C \int_{t_1}^{t_2} I_T dt} \quad \text{---------- (1)}$$

$$\eta = \frac{Q_u}{A_C I_T} = F_R(\alpha\tau) - F_R U_L \frac{(T_i - T_a)}{I_T} \quad \text{---------- (2)}$$

A cover and plate's radiative optical parameters and the total energy they received were related to efficiency. The loss coefficient UL represents the increase in temperature about the environment. FR was derived from the other parameters as a function of the removal factor. Natural convection dryer efficiency with reflectors is used to increase radiation on the collector as a result of orienting it from north to south. A typical January day in Bhavnagar, Gujarat, India, with peak solar irradiation, was the subject of the tests. A simulation of the dryer was conducted to compare the results obtained from a real dryer. There was a collector area of 1.85 m2 and a chamber capacity of 3.47kg. It was measured that the collector efficiency increased from 40.1% to 48.6% while the simulation showed that it increased from 36.6% to 50.4%. It was found that a dryer with a smaller collector area was more efficient [10]. An empirical exponential fit is used to analyze experimental data to study efficiency based on characteristic parameters. A chimney with a black plate painted black was placed at the end of the greenhouse to promote natural convection. In this study, it was observed that efficiency depends on inlet and outlet temperatures, air mass velocity, and incident solar radiation.

## 2. Methodology

A solar dryer (Figure 1) usually consists of an enclosure where the material to be dehydrated is placed, often in the form of a chamber or a tunnel. It can be an insulated enclosure with hot air intake and moist air exhaust ducts. A solar collector is the main source of energy for the process, which heats the air upstream of the enclosure.

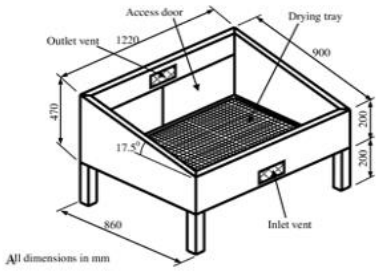


Fig. 1. Exploded view of the dryer modules

The two components that make up a dehydrator are the same. There are also air ducts, fans, heaters, control and measurement devices, and energy storage mechanisms that can be used for heating air or circulating air. It was decided to build coupled modules [11]. The collector and dehydration chamber sections were constructed from pine wood. An air pre-heater collection surface was constructed from a corrugated zinc sheet to maximize surface area. The different design variables were then coupled together. The three modules are depicted as follows: 2.47 m long and 0.83 m wide, 0.0003 m thick corrugated galvanized sheet metal, painted black, was used for the air pre-heater. The roof was constructed of pine wood with a 0.0255 m wide square section, insulated with 0.005 m thick plywood on the outside and plastic on the inside. There is a 0.2 m distance between the reader's internal base and the roof, with three PVC supports supporting the galvanised sheet metal in the middle. Polycarbonate was used for the transparent roof, with a 0.02 m thick anti-UV surface, and aluminum profiles were used to frame it [12]. To match the latitude of the site when mounted, it was angled at the same angle. This chamber consists of a 0.0256 m square section of pinewood framed in 0.0004 m thick iron sheeting, with an interior dimension of 0.82 m wide by 0.7 m deep. The junction with the preheater has a height of 0.4m, while the rear face has a height of 0.43 m, ensuring the roof of the chamber has an inclination equal to the site's latitude. The exterior was covered with 0.005 m thick plywood and insulated with 0.0255 m glass wool. The roofs were demountable and measured 0.82 m by 0.62 m each. A square-section pine frame was built with 0.005 m thick plywood on both sides and 0.0255 m thick glass wool in the middle [13]. It was framed in aluminum profiles with 0.02 m thick anti-UV alveolar polycarbonate sheets with the same surface as the first cover. A sheet metal chimney supports a 0.003 m thick iron structure with an internal diameter of 0.3m, supported by four pinewood trestle-type supports. The chimney has an elbow at 0.4m from the exit of the drying chamber and then a vertical section 1.3 m high, which is topped off by a wind extractor made up of two metal rings placed one on top of the other. By using parallel blades, the wind creates verticality when it passes through the space between them, causing the internal pressure to drop and the air to escape. The first prototype of the air heater is called mixed, and it consists of a collector, a drying chamber, and a chimney. The indirect prototype consists of a collector, a drying chamber covered with an opaque cover, and a chimney. Direct is the last of the three types, and it consists of a drying chamber covered with a transparent covering and a chimney. A heat balance is calculated using the three components described above: an air collector to preheat the fluid, a dehumidification chamber, and a chimney. The pre-heater and chamber control volumes are assumed to have uniform temperatures. There are seven different lengths of control volumes in the preheater [14]. There is an assumption that the drying chamber has a uniform temperature throughout its centred volume and that the stack has a single control volume, assuming the air temperature does not vary appreciably throughout. Analogous to an electrical circuit diagram, each of the system elements will be analyzed for heat balance.

The air in the collector uses energy to heat up, the collector plate accumulates energy and there is only unidirectional flow. In the upper cover of the collector, what is gained by conduction is lost by radiation to the open sky and convection by wind action; it is not considered energy storage, as seen in (3). The gain is due to convection with the circulating air and radiation from the metal plate. The symbol convention is shown in the annexed table. There is a radiative exchange between the sky and the surroundings, the sky temperature is 10°C lower than the ambient temperature. The coefficients representing the radiative loss depend on the temperatures of the objects exchanging energy as shown as an example in (4) where temperatures should be expressed in Kelvin. The convective exchange depends on the wind speed as shown in (5). To calculate the coefficients of convective interchange in the upper and lower channels of the collector, with the flow regime provided by the stack (Re < 2000 and Ra < 107), the Grashof and Reynolds numbers fulfil the condition: 0.1 < Gr/Re2 < 10. The Nusselt numbers considered are those corresponding to natural and forced flows, from which a combined Nusselt is obtained; from these expressions, the coefficient of convective interchange in the upper and lower channels of the collector can be cleared. convective volume ($hf$ = $Nu$k/D$h$) for the collector [15]. A function of the wetted perimeter of each of the flow channels is used in (6), (7), and (8) to calculate Re. It is most representative to calculate Ra using the collector length. The equation (6) is valid for laminar flow (Ra < 109) (Churchill and Chu correlation). For parallel plates with forced flow, one isolated and one under constant heat flux, Tan and Chapters equation (7) (Tan and Chapters correlation) is used, where Pr equals approximately 0.71. A global Nusselt is obtained by combining both equations.

$$\alpha\tau_{pc}A_cI = m_pc_{pp}\frac{dT_p}{dt} + \dot{m}_fc_{pf}(T_{i+1} - T_i)_f + h_{f-c}(T_f - T_c) + \dot{m}_fc_{pf^1}(T_{i+1} - T_i)_{f^1} + \left(\frac{A_bk_bh_v}{e_vh_v+k_b}\right)(T_b - T_a) + h_{r\,p-c}(T_p - T_c) \quad \text{---------- (9)}$$

$$h_{fcc}A_{cc}(T_{fc} - T_{cc}) + h_{r\,pc-cc}A_{cc}(T_{pc} - T_{cc}) = h_vA_{cc}(T_{cec} - T_a) + h_{r\,ece-cl}A_{cc}(T_{cce} - T_{ci}(T_a)) \quad \text{---------- (10)}$$

$$\alpha_t\left(\frac{A_t}{2}\right)(I_{dir} + I_{dif}) = +A_th_v(T_t - T_a) + A_th_{t-f}(T_t - T_f) \quad \text{---------- (11)}$$

$$A_t h_{t-f}(T_t + T_f) + A_t h_{r\,t-c}(T_t - T_d) = \dot{m}_f c_{pf}(T_t - T_d)_f$$

-------- (12)

$$N_{u_H} = (0.825 + 0.328 Ra_H^{\frac{1}{6}})^2 \quad \text{---------- (13)}$$

$$(T_o - T_i) = \frac{A_C F_R(\propto\tau) I_T}{\dot{m} c_p} - \frac{A_C F_R(\propto\tau) I_{th}}{\dot{m} c_p} \quad \text{---------- (14)}$$

$$I_{th} = U_L \frac{(T_i - T_a)}{\propto\tau} \quad \text{---------- (15)}$$

The calculation program used for each configuration (mixed, indirect, and direct) was SIMUSOL, which uses electrical circuit diagrams generated by Dia and solved by Scepter. The results of SIMUSOL are interpreted and displayed. Material characteristics were analyzed based on their optical and thermal properties. The input data used in each simulation correspond to radiation and ambient temperatures recorded on the test days. The prototype's air velocity was used as a control variable. Simulation results were compared with measured results by averaging the recorded velocity values.

## 3. Outcomes of the Simulation

The data obtained from the field experiments played a crucial role in influencing the parameters and outcomes of the simulation, and vice versa. Here's a breakdown of how this interplay likely occurred:

### *3.1 Calibration of Simulation Parameters*

The data collected during the field experiments provided real-world values for various parameters such as solar radiation, ambient temperature, wind speed, and other environmental conditions. These real-world measurements were likely used to calibrate and validate the parameters within the computational simulation model. Adjustments may have been made to ensure that the simulation accurately reflected the actual conditions experienced during the field experiments.

### *3.2 Validation of Simulation Results*

The direct measurements from the field experiments served as a benchmark or validation for the accuracy of the simulation results. If the simulation results closely matched the field measurements, it would indicate that the computational model accurately represents the physical behavior of the solar dryers in the given environmental conditions.

### *3.3 Identification of Discrepancies and Model Refinement*

Any discrepancies between the simulation results and the field measurements might have prompted a closer examination of the simulation model. Researchers may have iteratively refined the simulation parameters to minimize the differences between the simulated and measured values. This process helps enhance the reliability of the simulation model.

### *3.4 Insights into System Performance*

Data from the field experiments provided insights into the actual performance of the solar dryers in the specific conditions of the Colombian Caribbean Coast. These insights likely influenced the researchers' understanding of the critical factors affecting the thermal efficiency of the solar dryers, which, in turn, could have led to adjustments in the simulation model to better capture these factors.

### *3.5 Enhancement of Predictive Capabilities*

The integration of field data into the simulation model contributes to the model's predictive capabilities. The ability to accurately predict the performance of solar dryers under varying conditions is crucial for practical applications and future design improvements.

Overall, the back-and-forth relationship between field experiments and simulation activities allowed for a more comprehensive and accurate assessment of the solar dryers' thermal performance in the Colombian Caribbean Coast environment. This iterative process helps researchers refine their models and gain deeper insights into the behavior of the system under study.

## 4. Standard Methods for Evaluating Thermal Performance

### *4.1 ASABE Standards*

The American Society of Agricultural and Biological Engineers (ASABE) has developed some standards related to solar drying, such as ASAE S424, which provides guidelines for testing solar dryers. Limitations: These standards may not cover the full spectrum of solar dryer designs, and their applicability can be limited to specific regions or crops.

### *4.2 ISO Standards*

The International Organization for Standardization (ISO) has standards related to solar energy, but specific standards for solar dryers are lacking. Limitations: The broad focus of existing ISO standards may not address the nuanced requirements of solar dryer testing, leading to the need for more specialized guidelines.

### *4.3 NREL's System Advisor Model*

The National Renewable Energy Laboratory (NREL) has developed the System Advisor Model, which includes a solar drying module for evaluating the performance of solar dryers. Limitations: While SAM provides a sophisticated simulation tool, its application may be more suitable for larger-scale systems. It might not capture the intricacies of smaller, decentralized solar dryer designs.

### *4.4 Empirical Correlation*

Some researchers propose empirical correlations based on experimental data to estimate the thermal performance of solar dryers. Limitations: Empirical correlations may lack generality and might be specific to certain conditions or materials. They may not be applicable across a wide range of solar dryer designs and applications.

### *4.5 Efficiency Indices*

Several efficiency indices, such as thermal efficiency and energetic efficiency, have been proposed to evaluate the performance of solar dryers. Limitations: Different indices may focus on specific aspects of performance, making it challenging to choose a single metric that universally represents the overall efficiency of diverse solar dryer systems.

*4.6 Mathematical Models*

Computational models, such as mathematical and numerical simulations, aim to represent the thermal behavior of solar dryers. Limitations: The complexity of these models can be a barrier to widespread adoption, and their accuracy heavily relies on the availability and accuracy of input parameters.

*4.7 Local Climate-specific Guidelines*

Some studies suggest developing guidelines tailored to specific local climates and crop types. Limitations: While this approach acknowledges the diversity of conditions, it may result in a plethora of region-specific methodologies, hindering standardization on a global scale. In conclusion, the lack of globally accepted standards for evaluating solar dryer performance stems from the diversity of applications and contextual factors. While various proposals exist, they often come with limitations related to applicability, specificity, or complexity. Achieving a consensus on standard methods requires a balance between generality and specificity, considering the wide-ranging conditions under which solar dryers are deployed globally.

## 5. Geometrical Parameters of the Solar Dryer

*5.1 Solar Collector*

Dimensions: Specify the length, width, and height of the solar collector. For example, "The flat-plate solar collector has dimensions of 2 meters in length, 1 meter in width, and 0.15 meters in height." Tilt Angle: Indicate the angle of tilt for the collector. For instance, "The collector is inclined at an angle of 25 degrees from the horizontal plane." Orientation: Describe the orientation of the collector with respect to cardinal directions. For example, "The collector faces south at a 180-degree azimuth angle."

*5.2 Dehydration Chamber*

Dimensions: Specify the length, width, and height of the dehydration chamber. For instance, "The dehydration chamber measures 2.5 meters in length, 1.5 meters in width, and 1 meter in height." Number of Trays: If applicable, mention the number of trays or shelves inside the chamber and their dimensions. For example, "The dehydration chamber includes three trays with dimensions of 1 meter by 0.5 meters each." Insulation: Provide details on the insulation material and thickness used in the chamber walls.

*5.3 Chimney*

Dimensions: Specify the dimensions of the chimney, including diameter and height. For example, "The chimney has a diameter of 0.3 meters and a height of 3 meters." Describe the position of the chimney about the dehydration chamber. For example, "The chimney is located at the rear of the dehydration chamber."

*5.4 Distances*

Collector to Chamber Distance: Indicate the distance between the solar collector and the dehydration chamber. For example, "The distance from the collector to the dehydration chamber is 2 meters. "Airflow Path Length: If relevant, specify the length of the airflow path from the chamber to the chimney. For instance, "The airflow travels a distance of 4 meters from the dehydration chamber to the chimney."

## 6. Radiative Exchange and Convective Coefficients

*6.1 Radiative Exchange*

Radiative exchange refers to the transfer of heat energy through electromagnetic waves, such as infrared radiation. In a solar collector, this involves the absorption and emission of solar radiation. The absorber plate of a solar collector absorbs incoming solar radiation. The efficiency of this absorption process is influenced by the absorptivity of the material. The emitted radiation from the absorber plate is then directed towards the working fluid in the collector, heating it up. A common parameter used to characterize the ability of a surface to absorb and emit radiation is the emissivity (ε). A high emissivity means a surface is effective at both absorbing and emitting radiation, making it a good choice for an absorber plate in a solar collector.

*6.2 Convective Coefficients*

Convective heat transfer involves the transfer of heat through the movement of fluids (liquid or gas). Convective coefficients quantify the rate of heat transfer through convection and depend on factors like fluid properties and flow conditions. In a solar collector, the working fluid (often water or a heat-transfer fluid) is heated as it passes through the collector. Convective coefficients are crucial in determining how efficiently heat is transferred from the absorber plate to the fluid. The convective heat transfer coefficient (h) is a parameter that represents the efficiency of heat transfer between a solid surface and a fluid. It is influenced by factors like fluid velocity, temperature difference, and properties of the fluid. High convective coefficients enhance heat transfer efficiency. In an instant, for a solar collector to function effectively, a balance between radiative exchange and convective heat transfer is crucial. The collector's design, material properties, and the characteristics of the working fluid all impact the overall efficiency of the system. Engineers and designers often consider these coefficients when optimizing solar collector performance.

## 6. Results and Discussion

Figure. 2-5 shows the results for temperature, relative humidity, duct velocity, wind velocity, and radiation; the radiation is compared with a Hottel adjustment for clear days calculated on an inclined plane. The mixed heater test is shown as an example, and similar results are produced for

the other two configurations. The mixed and indirect collector outlet temperatures differ noticeably from those in the indirect mode. The ambient temperature in the direct mode configuration is approximately 45°C, whereas in the indirect mode configuration it is approximately 40°C. The maximum temperature difference between direct mode and ambient mode is 25°C. A comparison between the direct mode and the first two modes shows that the temperature at the collector outlet in the first two modes is practically the same, whereas the direct mode reaches 50°C at the collector outlet. A temperature's behavior is influenced by changes in radiation. Based on the relative humidity values in the three tests, there is a good difference between the relative humidity outside and within the chambers, which provides a good indication of the dehydration conditions for any product. In accordance with its temperature, the chamber achieves low humidity values [16]. A proportional relationship is observed between the velocity measurements in the collector and the chimney, with the chimney causing a greater drag as the wind speed increases. The mass flow in all configurations is proportional to this drag, reinforced by the buoyancy force provided by the heated air in the collector or chamber in the direct configuration. It was observed that passing clouds were present on the test days.

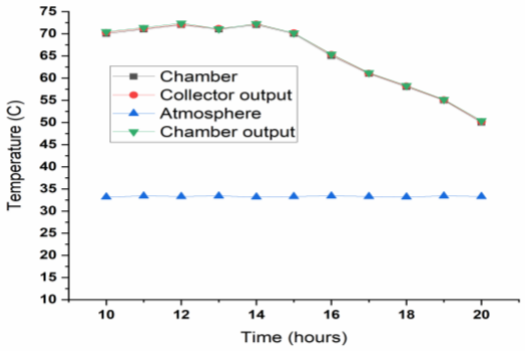


**Fig 2.** Measurements in the mixed dryer test, temperature

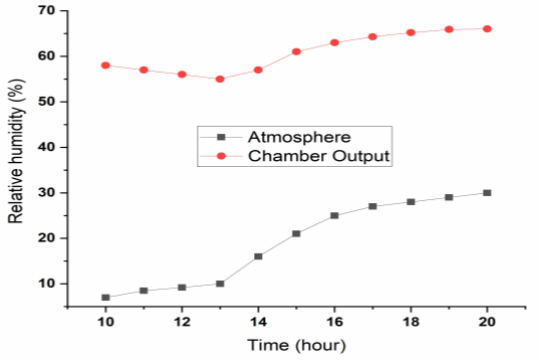


**Fig. 3.** Measurements in the mixed dryer test, relative humidity

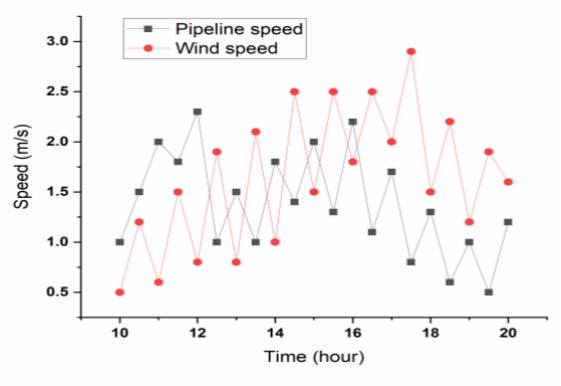


**Fig.** 4. Measurements in the mixed dryer test, relative humidity

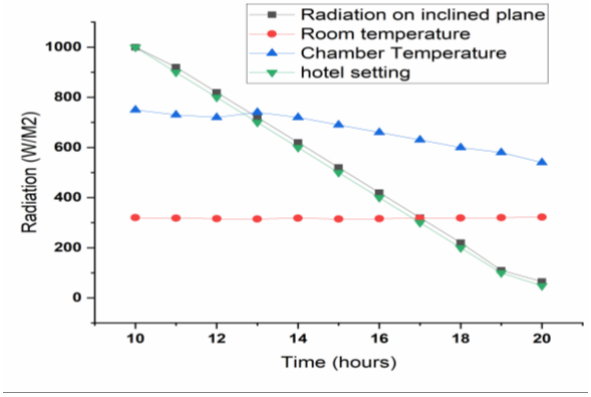


**Fig. 5**. Measurements in the mixed dryer test, radiation on inclined plane

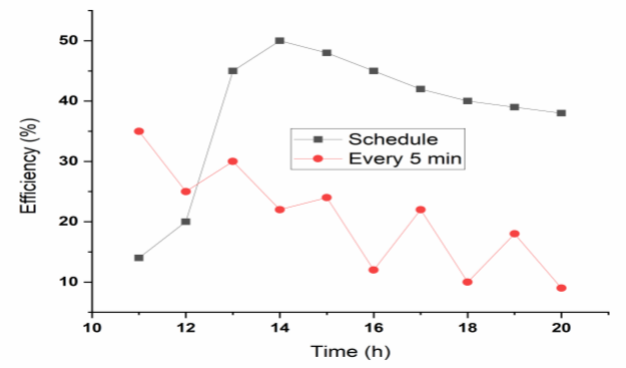


**Fig 6.** Thermal test results for mixed mode efficiency at different times

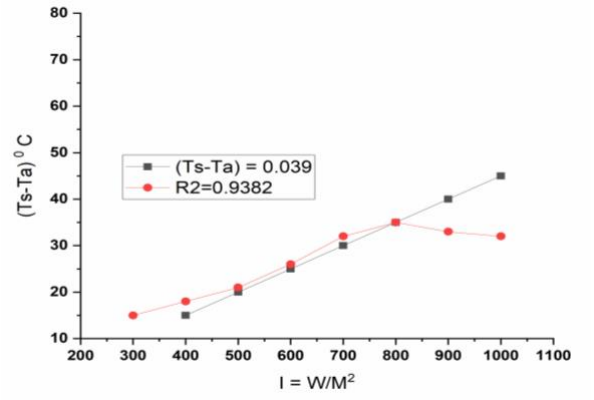


**Fig 7.** Thermal test results for mixed mode, temperature jump as a function of incident radiation.

In Figure 6, the hourly calculation is compared to the five-minute calculation to assess the thermal efficiency of the three heater configurations. As an example, five curves are generated for the mixed mode, and two curves are generated for the other two configurations. Based on the curve provided in the test, the average efficiency is calculated. In Figure. 6, the chamber outlet temperature difference is plotted as a function of incident radiation. The removal factor is then calculated using the average flux and collector area data [17]. The results of the tests are shown in Table 1.

**Table 1. Results of the analysis of the data provided by the field tests. Source: Authors**.

| Dryer type | Average flow rate (kg/s m2) | Collection area (m2) | Slope (°C/W/m2) $AcFR(\alpha\tau)$ $\dot{m}cp$ | Average efficiency in percent | Average |
|---|---|---|---|---|---|
| Mixed | 0.29 | 2.5 | 0.039 | 22 | 0.778 |
| Indirect | 0.17 | 2.0 | 0.031 | 18 | 0.453 |
| Direct | 0.05 | 0.5 | 0.015 | 1.2 | 0.258 |

The mixed mode shows a better thermal behaviour in comparison to the other two configurations, which is due to the difference in the collection area. Figure 7-9 shows the simulation results, comparing the outlet hot air temperatures with the actual measurements at the same position for three configurations. There is consistency between the test results and the simulation results. As average air and wind velocity values were used to calculate mass flow rate and external convective losses, over time the efficiency calculated by (1) oscillates around an average value due to variations in radiation. According to literature [18], the deviation of the simulation from the actual measurement is calculated by evaluating the standard deviation, standard error, and correlation coefficient.

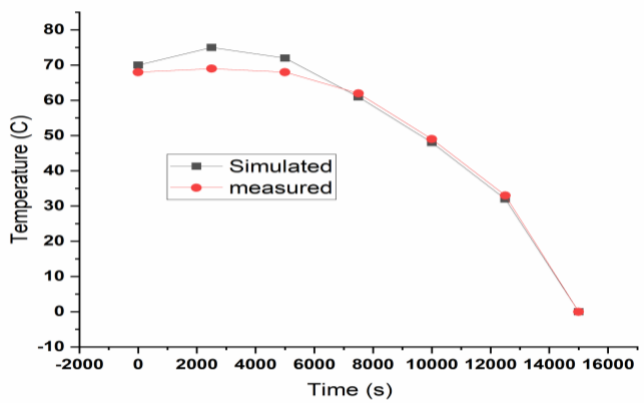


**Fig. 8.** Outlet temperatures. Simulated and measured. Mixed

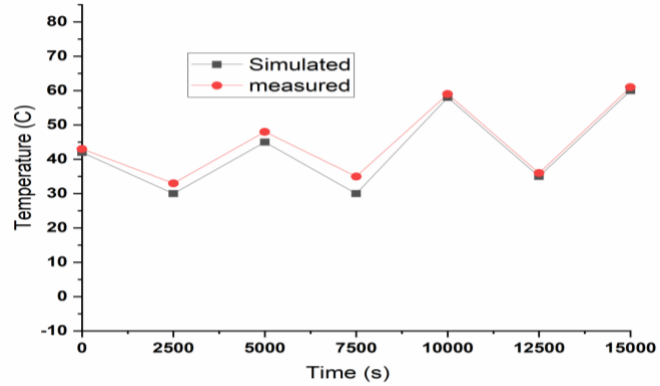


**Fig. 9.** Outlet temperatures. Simulated and measured. Indirect

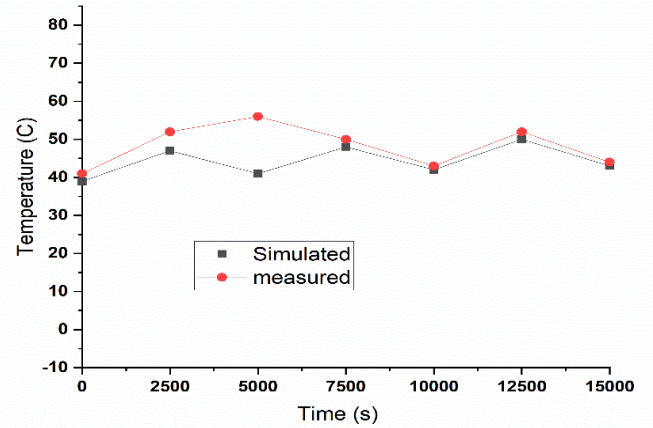


**Fig. 10.** Outlet temperatures. Simulated and measured. Direct

Table 2 shows the results obtained. Based on the fluctuations of solar radiation on the test days, it can be seen that the deviation in temperature in the chamber is statistically not very large. This result confirms that the simulation data matches the real values adequately. The low value of the standard error and the closeness of the correlation error to one support this claim [19]. A direct comparison was made between the heat required to heat a given mass of air and the radiant power reaching the transparent cover of each prototype, as shown in (2). Figure 10 shows the instantaneous efficiency calculated using the values produced by the simulation. The sharp variations occur due to variations in the intensity of radiation recorded in the plane of the transparent surface. The promised calculation shows consistency with the actual results, which show a mixed

configuration value of 44.3 %, an indirect configuration value of 32.5 %, and a direct configuration value of 25.5 %.

**Table 2. Statistical results of the comparison between real and simulated measurements for chamber temperature.**

| dryer | standard deviation | standard error | correlation coefficient |
|---|---|---|---|
| Mixed | 2.158 | 0.302 | 0.0981 |
| Indirect | 2.563 | 0.292 | 0.995 |
| Direct | 1.297 | 0.166 | 0.905 |

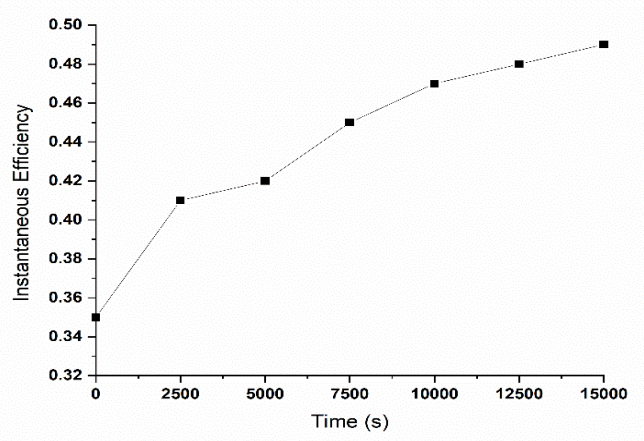


**Fig. 11**. Instantaneous efficiency. Mixed

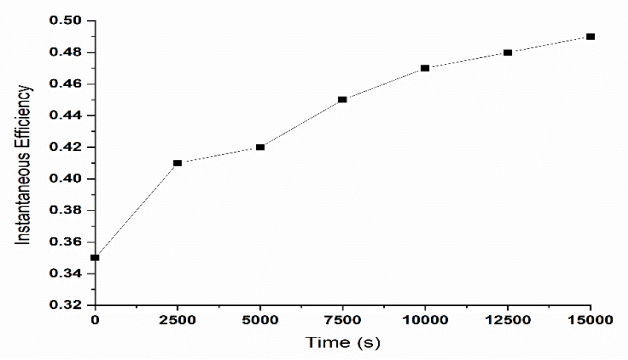


**Fig. 12.** Instantaneous efficiency. Indirect.

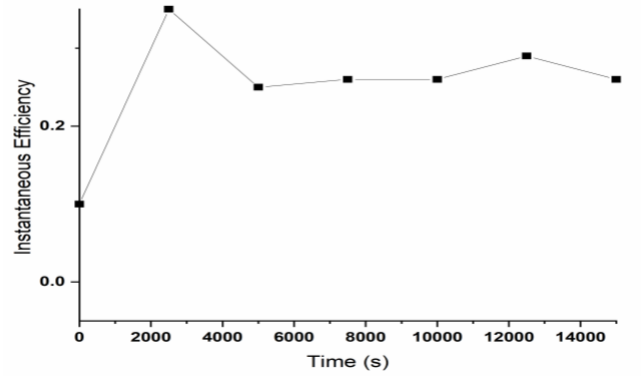


**Fig. 13.** Instantaneous efficiency. direct

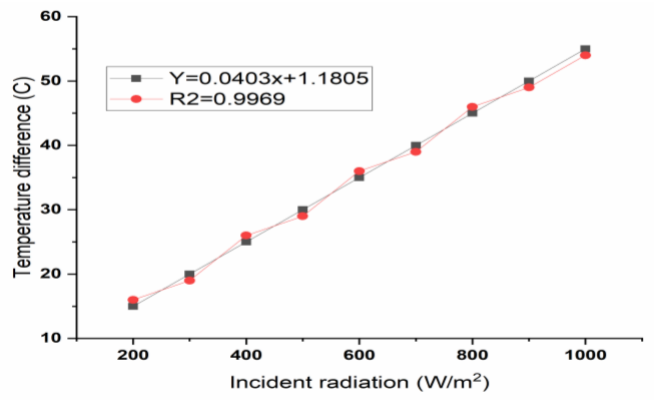


**Fig. 14.** Temperature difference between the chamber and the environment as a function of incident radiation. mixed.

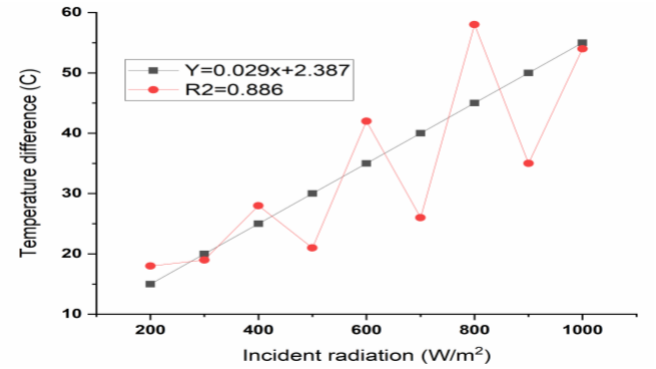


**Fig. 15**. Temperature difference between the chamber and the environment as a function of incident radiation. Indirect.

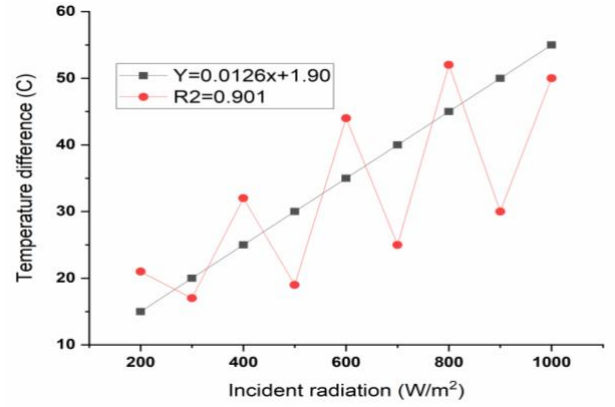


**Fig. 16.** Temperature difference between the chamber and the environment as a function of incident radiation. direct

The simulation calculated the temperature difference between the chamber and the environment. Based on the time values in the tables, only the values corresponding to the simulations themselves were taken, eliminating most spurious information and obtaining results similar to those calculated with measured data [19]. Temperature jumps were plotted as functions of incident radiation. The results are presented in Figure 11-16, where it can be seen that the test with the dryer in mixed mode produced a more significant linear fit compared to the other two configurations [20-22]. The test days are subject to varying levels of solar radiation. Based on the information provided by the linear fit between the differences, the removal factor was calculated for each prototype, taking into account the average flux values for

each data run and the constants used in each simulation. An average air density of 1.09 kg/m3 and a transmittance absorption ratio of 0.64 were used [23]. The slope of each dryer configuration varies markedly, since the area that collects radiation determines how much power reaches each configuration. The removal factor is determined by the simulation conditions. The trend is similar to what is observed when the same calculation is done with measured data.

**Conclusions**

In this paper, three configurations of solar dryers with natural air extraction regimes are compared in terms of their thermal behavior. The field tests were validated through a computational simulation using the data measured in different thermal tests carried out with the prototypes. A collector has two channels that are intended to circulate air in a circulating flow that is generated by a chimney and an extractor that generates wind velocity. The heat exchanges inside the collector, of convective and radiative type, as well as the heat losses through the roof to the environment, of convective and radiative type, and through the collector body to the environment, of conductive type in the collector body and convective type outside, are taken into account. A single airflow was assumed in the chamber as well. A buoyancy flow was produced by the chimney, coupled with variations in air density. In this simulation, the input values were ambient temperature, airflow, and solar radiation. The measured results were compared to the simulated results, which were compared to the measured results. Simulations were conducted using ambient temperature, airflow, and solar radiation as inputs; comparing measured results with simulations of solar radiation. The drying chamber, the efficiency as a collector, and the removal factor as an indicator of the average efficiency of each prototype are similar. There is a similarity between the removal factors and the efficiency curves. This type of thermal performance should be compared with those shown in the present work by using forced flow and air feedback in the same test protocol for all three configurations.

**References:**

[1] N.Rasaiah, R.Manickam, H.Ravikumar, J.R.Jegan, P.Nagarajan and K.Annadurai,"Comprehensive review on ideas, designs, and current techniques in solar dryer for food applications," Environ. Sci. Pollut. Res., vol. 30, pp. 93435–93461, 2023.

[2] A.Gupta, B. Das, A. Biswas and J. D. Mondol, "An environmental and economic evaluation of solar photovoltaic thermal dryer," Int J Environ Sci Technol, vol.19, pp. 10773–10792, 2022.

[3] P.Naveen, S.Dhanushkodi, and K.Sudhakar, "Eco-friendly drying techniques: a comparison of solar, biomass and hybrid dryers," Environ. Sci. Pollut. Res., vol. 30, pp.95086–95105, 2023.

[4] N. Kalaiselvan & M.Thangavel, "Design and fabrication of box-type passive solar dryer (BTPSD) with thermal insulation material for valorizing biomass and neutral lipids of marine Chlorella vulgaris for biodiesel application," Sci. Rep., vol.12, 6046, 2022.

[5] J. Aprajeeta, and P.P. Tripathy, "Recent Advancements in Design, Application, and Simulation Studies of Hybrid Solar Drying Technology," Food Eng. Rev., vol.13, pp.375–410, 2021.

[6] M.K.Admajith, B.T.Vaibhav, S.M.Arun, and N.T.Bhaskar, "Food Security and Sustainability Through Solar Drying Technologies: a Case Study Based on Solar Conduction Dryer," Mater. Circ. Econ., vol.4, 7, 2022.

[7] Z.Rong, Y.Qiongfen, L.Ming, X.Yiping, L. Aimin, Z.Danya, L.Yinning, and W.Yunfeng, "Experimental evaluation of a hybrid solar dryer with flexible open sorption thermal energy storage unit on demand for burdock root drying," Environ. Sci. Pollut. Res., vol.30, pp. 61977–61999, 2023.

[8] A. Karim and M. N. A. Hawlader, "Development of solar air collectors for drying applications," Energy Convers. Manag., vol. 45, pp. 329–344, 2004.

[9] S.Ankit, A.Abhishek, S.Amritanshu, K. Anil and S.Atul, "Performance evaluation of an industrial solar dryer in Indian scenario: a techno-economic and environmental analysis," Clean Technol Environ Policy., vol.24, pp. 2881–2898, 2022.

[10] H.Tanjum, T.Monika, B.Manaswita, and B.K.Shireesh, "Drying Kinetics, Quality and Economic Analysis of a Domestic Solar Dryer for Agricultural Products," INAE Letters, vol.4, pp.147–160, 2019.

[11] N.Manisha, T.Sumit, C.Deepak, K.Meena, T. Prabhakar, and K.S. Ravinder, "Recent developments on photovoltaic thermal drying systems: a clean energy production," Clean Technol Environ Policy., vol. 25, pp. 2099–2122, 2023.

[12] K.T.Amit, S.Rajesh, G.Anita, K.K.Ajay, A.Ronald, K.S.Subbarama, K.N.Sendhil and S.S.Vineet, "Advancements in solar technologies for sustainable development of agricultural sector in India: a comprehensive review on challenges and opportunities," Environ. Sci. Pollut. Res., vol. 29, pp. 43607–43634, 2022.

[13] A.Jain, M. Sharma, A. Kumar, A. Sharma and A. Palamanit, "Computational fluid dynamics simulation and energy analysis of domestic direct-type multi-shelf solar dryer," J. Therm. Anal., vol.136, pp.173–184, 2019.

[14] K.Baibhaw, K.R.Arun, S.Gábor, and S.Zoltán, "A conspectus review on solar drying of wood: regional and technical contrivances," J. Therm. Anal., vol.148, pp. 9237–9261, 2023.

[15] G. Duran, M. Condorí, and F. Altobelli, "Simulation of a passive solar dryer to charqui production using temperature and pressure networks," Sol. Energy, vol. 119, pp. 310–318, 2015.

[16] D.Mahesh, S.Kirti, and V. V. S. Murty, "The application of solar-driven technologies for the sustainable development of agriculture farming: a comprehensive review," Rev. Environ. Sci. Biotechnol., vol.21, pp.139–167, 2022.

[17] K. Mahesh, K.D.Ashwani, and K.S.Ravinder, "A comprehensive review of greenhouse shapes and its applications," Front. Energy,13, pp. 427–438, 2019.

[18] J.P. Holman, Experimental Methods for Engineers, 8th ed. New York: McGraw-Hill Education, 2011

[19] H. Merabet, T.Bahi, A.Boukadoum, and D. Drici, "Study and analysis of the operation of a Cuk converter for precise voltage regulation," ijSmartGrid, vol 7, pp. 148-153, 2023.

[20] L.Amira, B.Tahar, and I.Yousra, "Performance of Meta-heuristic Algorithm for a Photovoltaic System under Partial Shade," ijSmartGrid, vol. 7, pp. 160-167, 2023.

[21] P.K.Polamarasetty, S.S.N.Ramakrishna, V.Muddala, and M. Vinay Kumar, "A Review on The Estimate Solar PV Cell Variables For Efficient Photovoltaic Systems," ijSmartGrid, vol 7, pp. 154-159,2023.

[22] M. Kamruzzaman, Md. Anwarul, and Md. Anwarul Abedin, "Optimization of Solar Cells with Various Shaped Surficial Nanostructures," ijSmartGrid, vol 7, pp.113-118, 2023.

[23] A.T. Sofyan, D.Nael, and A.M. Anas, "Detection of xylene as a detrimental chemical compound by employing a photonic crystal based on porous silicon," ijSmartGrid, vol.7, pp.38-45, 2023.